Remote Sensing of Environment 117 (2012) 72–82

Contents lists available at ScienceDirect

Remote Sensing of Environment

journal homepage: www.elsevier.com/locate/rse

# Assessment of spectral, polarimetric, temporal, and spatial dimensions for urban and peri-urban land cover classification using Landsat and SAR data

Zhe Zhu [a,*], Curtis E. Woodcock [a], John Rogan [b], Josef Kellndorfer [c]

[a] Center for Remote Sensing, Department of Geography and Environment, Boston University, 675 Commonwealth Avenue, Boston, MA, 02215, USA
[b] Clark School of Geography, Clark University, 950 Main Street, Worcester, MA, 01610, USA
[c] Woods Hole Research Center, 149 Woods Hole Road, Falmouth, MA, 02540, USA

ARTICLE INFO

*Article history:*
Received 25 December 2010
Received in revised form 14 July 2011
Accepted 18 July 2011
Available online 28 September 2011

*Keywords:*
Classification
Landsat
SAR
Urban
Land cover

ABSTRACT

Urban and peri-urban environments are composed of a wide variety of materials, making land cover classification challenging. The objective of this research is to determine how effectively multi-season Landsat Enhanced Thematic Mapper Plus (ETM+) and single-season Advanced Land Observing Satellite (ALOS) Phased Array type L-band Synthetic Aperture Radar (PALSAR) data can be combined to map 17 land cover categories in the Greater Boston area of, Massachusetts, USA. The key goal of this work is to test the integration of radar and optical data. The contribution of different dimensions of input data to a random forest classifier was evaluated with map accuracy statistics. PALSAR data produced a 30.99% overall classification accuracy. Higher classification accuracy (72.24%) was achieved by adding texture variables derived from the PALSAR data. A September Landsat image produced a map accuracy of 77.96%. The inclusion of Landsat images from other three seasons increased map accuracy to 86.86% and Landsat derived texture variables further increased the map accuracy to 92.69%. The highest map accuracy (93.82%) was achieved by combining Landsat and PALSAR. Though combining PALSAR and Landsat only increased the overall accuracy by 1.1%, it was a statistically significant increase, whose magnitude was limited by the high accuracy already achieved with Landsat data. Moreover, confusion matrices and land cover maps indicated that most of this increase was from three urban land cover types (*low density residential*, *high density residential*, and *commercial/industrial*). The results demonstrate the value of combining multitemporal Landsat imagery, ALOS PALSAR data, and texture variables for land cover classification in urban and peri-urban environments.

© 2011 Elsevier Inc. All rights reserved.

## 1. Introduction

Image classification has a long history in the remote sensing community. It is the basis for many applications, such as carbon modeling, land use change, forest management, and crop yield estimation (Jung et al., 2006; Lark & Stafford, 1997; Wolter et al., 1995; Woodcock et al., 2001). Many classifiers have been developed and tested for land cover classification, such as maximum likelihood, neural networks, decision trees, support vector machines, and random forest (Breiman, 2001; Friedl et al., 2010; Gopal et al., 1999; Hansen et al., 2000; Huang et al., 2002; Lu & Weng, 2007; Strahler, 1980). The newly developed non-parametric classifiers generally perform better than the parametric classification methods (Huang et al., 2002), because their non-parametric nature can overcome limitations of multi-modal, noisy/missing data, and data with large and complex measurement spaces. Moreover, the relative importance of input variables can be investigated and modified to improve performance of specific land cover categories (Rogan et al., 2008). In spite of the advancement made in remote sensing classification, land cover map accuracy tends to be lower in urban environments relative to forest/grassland environments (Rogan & Chen, 2004). To improve urban land cover classification accuracy further, the largest benefits are likely to come from improving the inputs to the classifiers, rather than improving the classification algorithms.

Inputs from optical sensors are widely used in land cover classification due to the rich information content of the multispectral data. While most research has concentrated on the spectral dimension of the optical data (Bischof, et al., 1992; Bruzzone et al., 2006; Huang et al., 2002; Shimabukuro & Smith, 1991; Strahler, 1980; Wang, 1990), the temporal and spatial dimensions are addressed much less (Rogan & Chen, 2004). Temporal information has proven beneficial for improving classification accuracy, especially for vegetation, because of the differences in phenology associated with different vegetation types (Defries & Townshend, 1994; Friedl et al., 2010; Gopal et al., 1999; Guerschman et al., 2003; Hansen et al., 2000; Tucker et al., 1985; Wolter et al., 1995). Multitemporal data are one of the main inputs for large area land cover map products derived from the Advanced Very High Resolution Radiometer (AVHRR) and Moderate

* Corresponding author. Tel.: +617 233 6031.
*E-mail address:* zhuzhe@bu.edu (Z. Zhu).

0034-4257/$ – see front matter © 2011 Elsevier Inc. All rights reserved.
doi:10.1016/j.rse.2011.07.020

Resolution Imaging Spectroradiometer (MODIS) sensors (Friedl et al., 2010; Gopal et al., 1999; Hansen et al., 2000; Tucker et al., 1985). Defries and Townshend (1994) used the monthly NDVI values in global land cover mapping with AVHRR data. Wolter et al. (1995) reported a significant improvement when multitemporal Landsat Thematic Mapper (TM) images were used to map forest types in the northern lake states. Guerschman et al. (2003) explored how many dates, and the best combinations of Landsat TM images needed to obtain accurate land cover map in the Argentine Pampas.

The spatial dimension of remote sensing images as measured by image texture contains information on local spatial structure and variability of land cover categories, and can increase land cover classification accuracies in heterogeneous landscapes (Ghimire et al., 2010). Texture information has improved classification accuracy for optical sensors such as the Satellite Pour l'Observation de la Terre (SPOT) High Resolution Visible (HRV) sensor (Franklin & Peddle, 1990; Steven & Derek, 1990), Landsat TM (Chica-Olmo & Abarca-Hernandez, 2000), Multispectral Electro optical Imaging Scanner (MEIS-II) (Anys et al., 1994), and airborne multispectral sensors (Franklin, et al., 2000). The optimal window size for texture measurements is highly dependent on the image spatial resolution and the land cover characteristics (Pesaresi, 2000). Generally, window size should be large enough to include the entire texture pattern, and at the same time small enough to include only one land cover type (Dell'Acqua & Gamba, 2006; Pesaresi, 2000; Puissant et al., 2005). Shaban and Dikshit (2001) computed texture measurements with different window sizes as inputs for urban area classification using SPOT HRV. They suggested window sizes of $7\times7$ and $9\times9$ pixels performs best and beyond this the accuracy may slightly increase or decrease but the difference is not statistically significant.

Synthetic Aperture Radar (SAR) sensors are playing an increasingly important role in remote sensing due to their ability to operate day and night through cloud cover, and recent improvement in data availability (Rogan & Chen, 2004). Many studies have focused on the spectral and polarimetric dimensions of SAR data in land cover classification (Chen et al., 2003; Cloude & Potter, 1997; Lee, et al., 1994), whereas SAR image texture is found helpful in improving map accuracy, particularly for urban and forest categories (Dekker, 2003). The textures offered by SAR images are more appealing considering the inherent speckle noise that makes single pixel value unreliable. Though SAR images have long been limited in their use for urban characterization due to their sensitivity to clustered and irregular urban structures, SAR texture measures can provide valuable information (Dekker, 2003; Dell'Acqua & Gamba, 2003). The isolated scattering residential areas are quite different from town centers with lots of crowded backscatters or financial areas, where some of the high buildings cause peaks in SAR response (Dell'Acqua & Gamba, 2006). Simard et al. (2000) found texture measures from Japanese Earth Resources Satellite-1 (JERS-1) are important features for the differentiation of flooded vegetation in Central Africa. Ulaby et al. (1986) reported the use of SAR texture information ($8\times8$ pixels suggested as the optimal window size) improved overall land cover accuracy with Seasat SAR data acquired over northeastern Oklahoma and provided better mapping of forest types with Shuttle Imaging Radar-A (SIR-A) SAR data acquired over forested areas in North and South America. Additionally, multitemporal SAR images have also proven useful in urban, forest, and agriculture land cover classification (Le Toan et al., 1989; Pellizzeri et al., 2003; Quegan et al., 2000; Schotten et al., 1995).

Recent studies report that the integration of optical and SAR data might be beneficial due to their distinct features. Optical images contain information on surface reflectance and emissivity characteristics, while SAR images capture the structure and dielectric properties of the Earth surface materials. Land cover types that are impossible to separate in optical images might be distinguishable with SAR images and vice versa because of the complementary information contained in the two datasets (Amarsaikhan & Douglas, 2004). Many approaches employing both optical and SAR images have been explored for land cover classification (Amarsaikhan & Douglas, 2004; Blaes et al., 2005; Chust et al., 2004; Corbane et al., 2008; Kuplich et al., 2000; Michelson et al., 2000; Rott, 1994; Shupe & Marsh, 2004; Solberg et al., 1994; Toll, 1985). The results from integrating optical and SAR sensors are always significantly higher than those obtained from using an individual sensor, particularly for certain land cover types, such as urban (Corbane et al., 2008; Toll, 1985), agriculture (Blaes et al., 2005; Chust et al., 2004), wetlands (Augusteijin & Warrender, 1998; Li & Chen, 2005), and desert vegetation (Shupe & Marsh, 2004).

The objective of this study is to quantify the importance of the different dimensions (spectral, polarimetric, temporal, and spatial) of the input data, and the best accuracy achievable by combining optical and SAR sensors in urban and peri-urban land cover classification. We first explored the importance of the polarimetric and spatial dimensions provided by PALSAR images alone. Then, the contributions of the spectral, temporal, and spatial dimensions in Landsat were assessed. Finally, we integrated both Landsat and ALOS data to create the best land cover map with all the available dimensions and analyzed the importance of the variables from the different dimensions.

## 2. Data and study area

### 2.1. Study area

The study area is located in Eastern Massachusetts (Fig. 1) and covers 12,404 $km^2$. Approximately half of the study area is dominated by mixed temperate forest consisting of broadleaf deciduous trees (e.g., red maple-*Acer Rubrum*, sugar maple-*Acer Saccharum*, beech-*Fagus*, and oak-*Quercus*), as well as white pine-*Pinus strobus* and eastern hemlock-*Tsuga canadensis*. The non-forested portion of the study area is largely composed of agricultural and urban land uses. The study area has a subtle elevation gradient ranging from sea level in the east to 500 m in the west. The climate is mild with an average annual temperature of 8.8 °C. Average annual precipitation for the study area is 115–130 cm (NCDA, 2008) and the dominant soil type is coarse sandy loam.

The dominant land change in the last 20 years has been forest loss due to urban sprawl (DeNormandie, 2009), a common pattern of forest loss across North America (Butler, 2008; Nowak & Walton, 2005). Recent estimates suggest that Massachusetts loses roughly 16 ha of forest per day due to urban sprawl, which is concentrated primarily in Southeastern Massachusetts and along the Interstate Highway 495 corridor (Breunig, 2003; Davis, 2007; DeNormandie, 2009). These diverse land covers provide a good opportunity to test the value of different remote sensing inputs to land cover classification.

### 2.2. Landsat data

Four Landsat ETM+(Path 12 Row 31) images from different seasons prior to the Scan Line Corrector (SLC) failure were chosen as the optical input data. The Landsat image classified first was captured on September 27th 2000 (autumn). Next, three images from other seasons (a winter image from December 3rd 2001, a spring image from April 10th 2002, and a summer image from June 29th 2002) were added in sequence to test the effect of multitemporal inputs. To reduce the effect of the atmosphere, the raw DN values were converted to surface reflectance (Fig. 2a) with the Landsat Ecosystem Disturbance Adaptive Processing System (LEDAPS) atmosphere correction tool (Masek et al., 2006; Vermote et al., 1997).This atmosphere correction algorithm uses the MODIS 6S radiative transfer approach in retrieving surface reflectance. The thermal band was converted to brightness temperature and resampled to 30 m. Cloud and cloud shadows (less than 1% of the each scene) were masked using an object based method (Zhu & Woodcock, submitted for

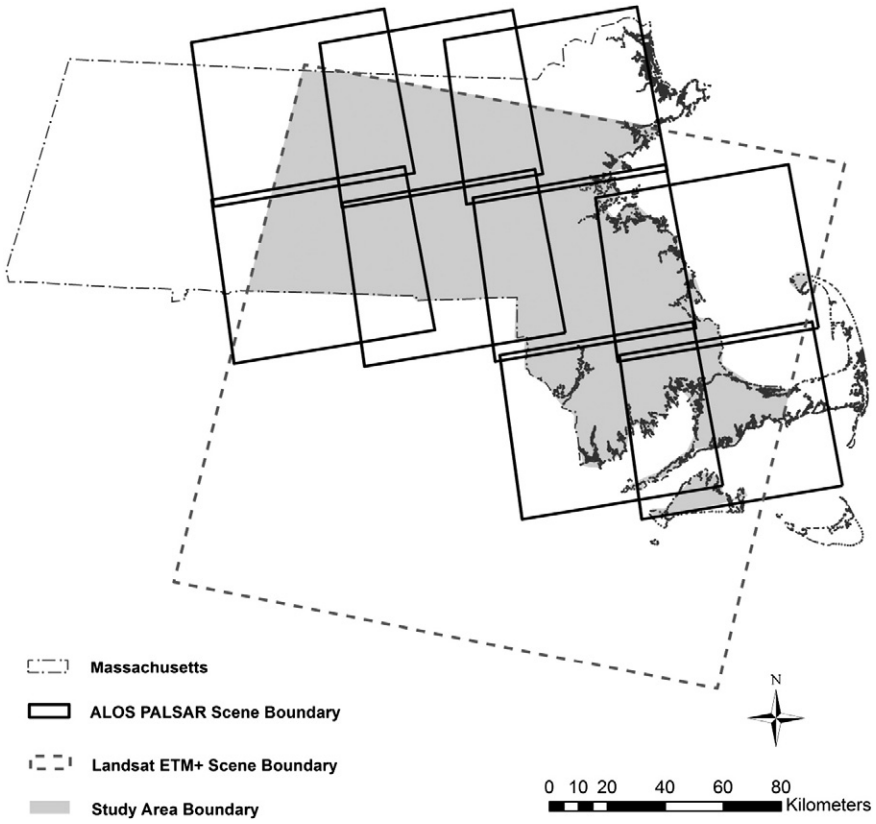


**Fig. 1.** Study area.

publication). Pixels that had clouds or shadows in any of the Landsat images were excluded from further analysis.

### 2.3. PALSAR data

The L-band ALOS PALSAR data (Rosenqvist et al., 2007) used in this study were acquired in the Fine Beam Dual (FBD) mode, i.e., dual polarization HH (horizontal-horizontal) and HV (horizontal-vertical), with an incidence angle of 39 degrees and a pixel spacing of 9.4 m (slant range) by 3.2 m (azimuth). The data were acquired from the American ALOS Data Node at the Alaska Satellite Facility (ASF-AADN) and processed with the Woods Hole Image Processing System (WHIPS). Processing steps were (1) multi-looking Single Look Complex Data converted to 4 look multi-look detected data; (2) application of a Gamma MAP speckle filter in slant range format (Baraldi & Panniggiani, 1995); (3) orthorectifictaion and local incidence angle correction during geocoding (Kellndorfer et al., 1998; SARScape User Manual, 2009); and (4) conversion of power data to 8bit dB units to generate a three-band composite of L-band HH, LHV, and the ratio of HH/HV. A total of nine ALOS PALSAR scenes acquired between June and July 2007 were mosaicked. The final mosaic was a 24-bit GeoTIFF image with a pixel resolution of 15 m in Albers Equal Area Projection. For integration with the Landsat data in this study, the PALSAR data were reprojected to the UTM coordinate system (WGS 84 datum) and resampled to 30 m using nearest neighbor interpolation. Two kinds of PALSAR images were used here — the unfiltered (without the speckle filter) and the filtered versions. To better preserve the texture of the PALSAR images, we used the unfiltered PALSAR images (Fig. 2b) for texture computing, and used the filtered version of the images (Fig. 2c) directly for land cover classification.

### 2.4. Ground reference data

Ground data were previously used to calibrate the HERO Massachusetts Forest Monitoring Program (MaFoMP) 2000 land cover product (Rogan et al., 2010). Ground data were created with the aid of aerial photographs and fieldwork from 2005 to 2007. Orthorectified true color aerial photographs representing leaf-off conditions in April 2005 were acquired from MassGIS (2009). These data were captured by Sanborn LLC using a Vexcel Ultracam digital camera at an altitude of 1545 m and have a spatial resolution of approximately 45 cm. All ground data were $60 \times 60$ m in dimension, and were distributed throughout the study region to capture variation in reflectance values across the study area. There are 17 land cover categories with a total of 10,502 reference locations in Massachusetts (Table 1 and Fig. 3). A total of 5,485 reference locations are in the study area.

## 3. Methods

### 3.1. Classifier

A Random Forest Classifier (RFC) was used to create land cover maps of the study area and test the influence of different input variables on map accuracy. The term random in RFC signifies random selection of a certain proportion of training data as well as random selection of a user defined number of splitting variables and the term forests implies that a collection of trees are generated using the algorithm. The RFC is a non-parametric classifier that uses an ensemble of tree based classifiers $\{h(x, \Theta_k), k = 1, \ldots\}$ where x is the input vector and $\Theta_k$ are the independent identically distributed random vectors (Breiman, 2001). A large number of classification trees can be generated using bootstrap samples with replacement from the training data. Pixels are assigned to each class based on a majority voting rule which assigns a pixel to the class that receives the maximum number of votes from the group of classification trees. For example, suppose there are two classes A and B and out of 100 classification trees built, 60 trees classify a pixel as class A and 40 trees classify that same pixel as B. In this case the pixel is assigned to class A as more trees predict category A. Each tree is trained using a certain percentage of randomly selected training samples with the remaining

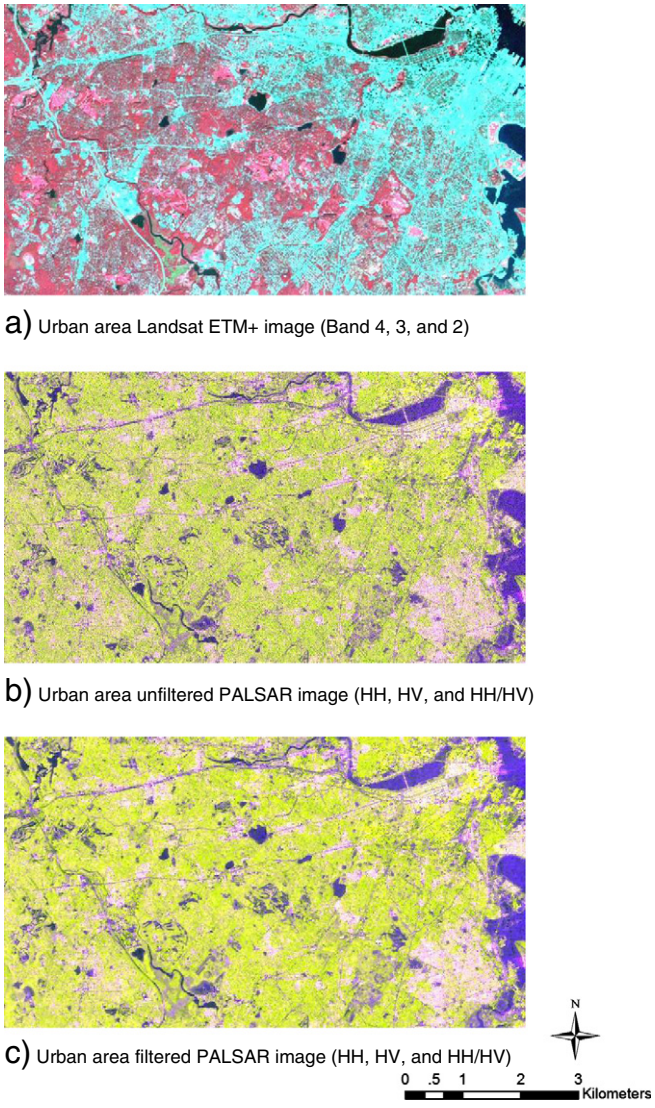


**Fig. 2.**

**Table 1**
17-categories land cover description.

| Class | Description |
|---|---|
| Orchards | Managed plantation of fruit trees, primarily apples |
| Cranberry bogs | Managed bog containing cranberry bushes, seasonally flooded |
| Pasture/row crops | Open and cultivated agricultural grasslands |
| Deciduous forest | Forested land ≥ 80% broadleaved deciduous canopy cover |
| Conifer forest | Forested land ≥ 80% needleleaved evergreen canopy cover |
| Mixed forest | Forest land > 20% conifer and < 80% deciduous canopy cover |
| Golf course | Highly managed open grasslands |
| Grassland | Grassland dominated open spaces |
| Low density residential | Residential land with equal parts impervious surface and vegetation |
| High density residential | Residential land minimally vegetated, > 60% impervious surface |
| Commercial/industrial | Impervious surface |
| Deep water | Standing deep water present > 11 months |
| Shallow water | Standing shallow water present > 11 months |
| Wetland | Vegetated lands with a high water table |
| Salt marsh | Tidal saltwater rivers/mudflats and surrounding herbaceous cover |
| Sand quarry | Sand and gravel mining pits |
| Bare soil | Bare land sparsely vegetated, > 60% soil background |

percentage of training samples, called "out-of-bag" samples, serving to estimate the classification accuracy. In addition, the best split at each node can be obtained by a user defined fixed number of feature variables that can be randomly selected from the group of feature variables.

The RFC has the advantages inherent to classification trees because it uses classification trees as the base classifier (Breiman, 2001). In addition, the RFC is easy to use and operate because only two input parameters have to be adjusted (i.e., the number of trees and number of split variables at each node). Optimal results can be obtained by selecting the number of trees and the number of split variables that provide the smallest out-of-bag error rate. Usually, the larger the number of trees, the higher the accuracy, and the upper limit of trees depends on the computation time. The default value for the number of split variables is the square root of the total number of variables, and its "optimal" range is usually quite wide. Furthermore, the results from RFC are not hampered by the problem of overfitting because the large number of trees generated ensures generalization of the patterns in the data (Breiman, 2001). RFC has been used in applications related to land cover classification (Gislason et al., 2006; Ham et al., 2005; Pal, 2005) and landscape ecology (Prasad et al., 2006). In this study, a total of 500 trees were grown for each classification scenario, and the square root of the number of total input variables were used as the number of split variables at the nodes.

Variable importance was estimated by the difference in prediction accuracies between the permuted and original out-of-bag samples (Breiman, 2001). Although the structure of a classification tree contains information about every important variable, this kind of interpretation is impossible for RFC which utilizes hundreds of trees in an ensemble. To estimate the importance of the *m*th variable, the out-of-bag samples of the *m*th variable are randomly permuted first (breaking the predictor variable's original association with response Y). Next, the permuted out-of-bag samples are run through all the Random Forest trees again. Finally, the variable importance is computed by averaging the difference in accuracies between the original and the permuted out-of-bag samples for all the trees. The merit of the Random Forest variable importance measure compared to univariate screening methods is that it not only includes the influence of each predictor variable separately but also the multivariate interactions with other predictor variables, which make this advanced approach more efficient and accurate (Breiman, 2001; Gislason et al., 2006; Chan & Paelinckx, 2008; Archer & Kimes, 2008).

### 3.2. Maps accuracy evaluation

We performed a fifty-fold cross-validation analysis with the training database. A total of 80% of the ground reference data were randomly selected to train the classifier, and the remaining 20% were used to assess map accuracy (Fielding & Bell, 1997). This process was repeated 50 times and we use the average overall classification accuracy to compare the results for different combinations of input data. The confusion matrices, producer's accuracy, and user's accuracy were calculated using the remaining 20% for three scenarios (Scenario 2, 7, and 8 in Table 2).To quantitatively evaluate the efficiencies in classification accuracies, a Paired *t*-test was performed. For each classification scenario there are fifty map accuracy results, and the Paired *t*-test of the accuracies tests whether the observed increase in the mean overall accuracy is statistically significant (at the 95% level).

## 4. Results

### 4.1. Inputs from PALSAR

We explored the polarimetric and spatial dimensions of the SAR data. The use of the L-band dual polarization (HH and HV) PALSAR

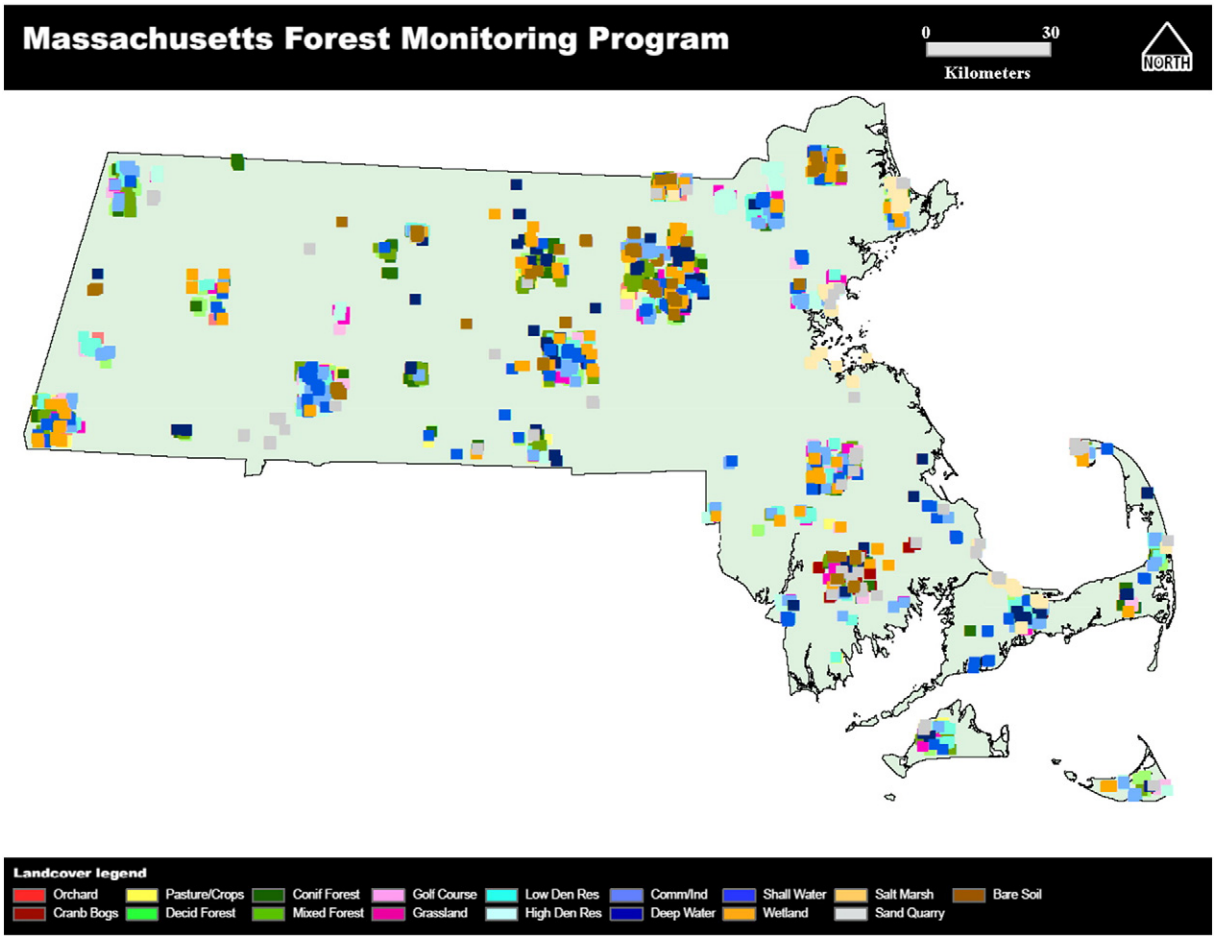


**Fig. 3.** 17-categories land cover reference map of Massachusetts.

images (Scenario 1 in Table 2) resulted in low overall land cover mapping accuracy (30.99% in Fig. 4).

In the spatial dimension, eight texture variables (9×9 pixels window size) for HH and HV bands were created using Grey-Level Co-occurrence Matrix (GLCM) measures (Franklin & Peddle, 1990; Gong & Howarth, 1992), including the mean, variance, homogeneity, contrast, dissimilarity, entropy, second moment, and correlation (Lu & Batistella, 2005). The overall map accuracy increased to 72.44% when the texture data were combined with the dual polarization bands (Scenario 2 in Table 2). Results of the Paired *t*-test indicated that this improvement was statistically significant at the 95% level.

The confusion matrix for the land cover classification derived from PALSAR polarimetric and spatial dimensions is presented in Table 3. Three urban land cover categories (*high density residential, low density residential*, and *commercial/industrial*) exhibited different map accuracies. Relatively high producer's (80.83%) and user's (74.68%) accuracies were observed for *high density residential*, while the producer's and user's accuracies for *low density residential* and *commercial/industrial* were below average (approximately 70% or less). The confusion matrix also illustrated the value of PALSAR data for distinguishing forest types. The producer's and user's accuracies for *deciduous forest*, *conifer forest*, and *mixed forest* were all higher than 70%. High producer's accuracy and user's accuracies (approximately 80% or higher) were achieved for *deep water* and *salt marsh*. The producer's accuracies for *cranberry bogs*, *pasture/row crops*, and *golf course* were approximately 60% or lower suggesting significant omission error for these three land cover types. The user's accuracies for *sand quarry* and *bare soil* were less than 60%, meaning large commission error in these land cover types. The land cover map derived from the PALSAR polarimetric and spatial dimensions (Scenario 2 in Table 2) exhibited many problems (Fig. 4a). Large areas of *shallow water* (Charles River and Boston bay area) were misclassified as *bare soil*. The *Low density residential* class was frequently misclassified as *conifer forest* and *mixed forest*. *Commercial/industrial* was sometimes misclassified as *high density residential* in downtown Boston. Moreover, *deciduous forest* tended to be falsely identified as *conifer forest* and *mixed forest*.

**Table 2**
Different scenarios of input variables for land cover classification.

| Scenario number | Number of variables | Name of variables |
|---|---|---|
| 1 | 2 | HH and HV PALSAR |
| 2 | 18 | HH, HV, HH textures, and HV textures PALSAR |
| 3 | 7 | Autumn Landsat |
| 4 | 13 | Autumn and winter Landsat |
| 5 | 19 | Autumn, winter and spring Landsat |
| 6 | 25 | Autumn, winter, spring and summer Landsat |
| 7 | 73 | Four seasons Landsat and autumn Landsat textures |
| 8 | 91 | HH, HV, HH texture, HV texture, four seasons Landsat and autumn Landsat textures |

### 4.2. Inputs from Landsat

All seven spectral bands (including the thermal band) in the autumn (September) Landsat image were used to explore the spectral dimension (Scenario 3 in Table 2). The overall classification accuracy

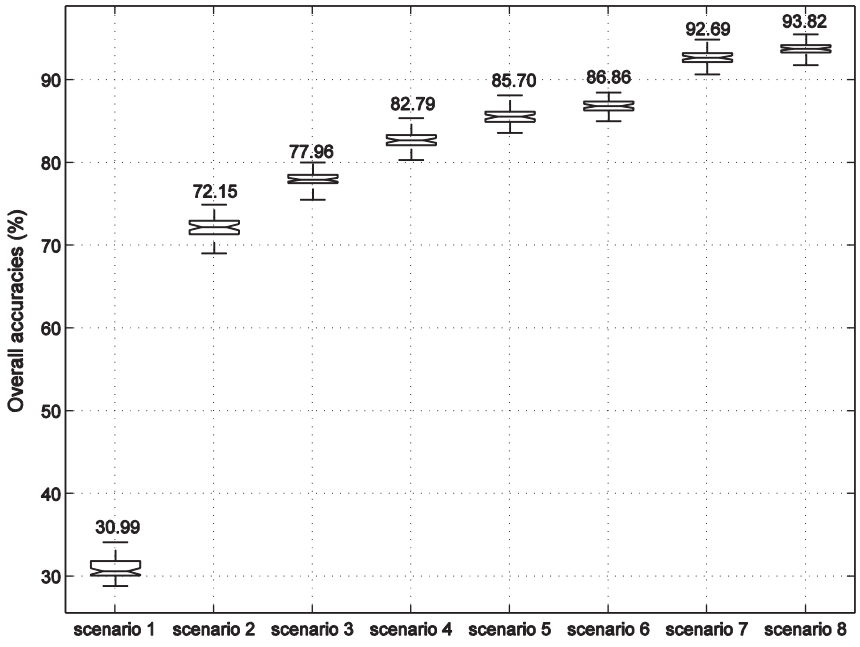


**Fig. 4.** Overall classification accuracies with different inputs (refers to Table 2).

from this single-date Landsat image (77.96%) was more than 5% higher than the best accuracy (including texture variables) obtained using PALSAR data (Fig. 4).

Three additional Landsat images from different seasons were combined to explore the temporal dimension (Fig. 4 and Scenario 4–6 in Table 2). We only added the multitemporal visible, near-infrared (NIR), and Short Wave Infrared (SWIR) bands for land cover classification. The thermal bands from the other three seasons were not included here because multitemporal thermal bands did not improve classification results. The Paired *t*-test indicated that adding multitemporal thermal bands did not increase classification accuracy at the 95% significance level. In general, there is not much information contained in multitemporal thermal data as temporal changes are mostly the result of seasonality, which is common to all land covers. Winter (December), spring (April), and summer (June) Landsat images were added sequentially to the original Landsat autumn (September) image. An approximate 7% increase in map accuracy (map overall accuracy of 86.86%) was achieved by using Landsat images from all four seasons. The largest increase in overall accuracy was achieved through the addition of a snow free winter (December) image to the autumn (September) image. Paired *t*-test suggested that each scenario was statistically significant different from the previous scenario at the 95% level.

For each spectral band (except the thermal band) of the autumn (September) Landsat image, eight texture variables (9×9 window) were calculated using GLCM measures to test the value of the spatial dimension (Scenario 7 in Table 2). The window size for calculating the texture variables was 9×9 pixels. The addition of the spatial dimension resulted in an almost 6% increase in overall accuracy. By using all the available dimensions of Landsat data (spectral, temporal, and spatial), the best land cover map obtained an overall accuracy of 92.69%. Paired t-tests between this accuracy and the accuracy derived

**Table 3**
Confusion matrix for 17-categories land cover classification derived from PALSAR dual polarization bands and their texture measures.

| | O | CB | PC | DF | CF | MF | GC | G | LD | HD | CI | DW | SW | W | SM | SQ | BS | Tot. | User |
|---|---|---|---|---|---|---|---|---|---|---|---|---|---|---|---|---|---|---|---|
| O | 1573 | 23 | 162 | 1 | 13 | 4 | 22 | 37 | 14 | 0 | 70 | 0 | 9 | 161 | 52 | 57 | 6 | 2204 | 71.37 |
| CB | 16 | 1592 | 152 | 0 | 0 | 0 | 70 | 44 | 0 | 0 | 18 | 13 | 33 | 9 | 63 | 86 | 48 | 2144 | 74.25 |
| PC | 160 | 182 | 2388 | 16 | 0 | 7 | 95 | 110 | 74 | 0 | 67 | 33 | 148 | 48 | 111 | 57 | 66 | 3562 | 67.04 |
| DF | 1 | 0 | 3 | 2746 | 102 | 740 | 0 | 5 | 78 | 2 | 8 | 0 | 0 | 79 | 0 | 19 | 0 | 3783 | 72.59 |
| CF | 14 | 0 | 8 | 96 | 3054 | 615 | 0 | 0 | 67 | 32 | 2 | 0 | 0 | 5 | 0 | 8 | 0 | 3901 | 78.29 |
| MF | 1 | 13 | 32 | 362 | 339 | 4569 | 0 | 10 | 88 | 0 | 12 | 0 | 0 | 29 | 0 | 0 | 0 | 5455 | 83.76 |
| GC | 34 | 58 | 175 | 0 | 0 | 1 | 1822 | 111 | 32 | 4 | 210 | 26 | 108 | 55 | 0 | 76 | 33 | 2745 | 66.38 |
| G | 22 | 119 | 187 | 13 | 0 | 7 | 174 | 2217 | 70 | 13 | 196 | 40 | 93 | 46 | 54 | 97 | 59 | 3407 | 65.07 |
| LD | 23 | 0 | 20 | 66 | 136 | 143 | 4 | 45 | 2153 | 188 | 131 | 0 | 0 | 186 | 0 | 0 | 1 | 3096 | 69.54 |
| HD | 1 | 0 | 0 | 7 | 90 | 0 | 8 | 0 | 238 | 1,324 | 69 | 0 | 0 | 11 | 0 | 25 | 0 | 1,773 | 74.68 |
| CI | 79 | 0 | 94 | 29 | 30 | 16 | 152 | 249 | 154 | 70 | 2353 | 40 | 44 | 97 | 22 | 63 | 39 | 3531 | 66.64 |
| DW | 0 | 6 | 30 | 0 | 0 | 5 | 40 | 104 | 0 | 0 | 18 | 3572 | 442 | 0 | 0 | 10 | 30 | 4257 | 83.91 |
| SW | 5 | 56 | 46 | 0 | 2 | 0 | 73 | 108 | 32 | 0 | 60 | 646 | 2,371 | 17 | 1 | 38 | 59 | 3,514 | 67.47 |
| W | 100 | 61 | 70 | 94 | 39 | 129 | 73 | 36 | 146 | 0 | 42 | 2 | 48 | 2272 | 1 | 31 | 22 | 3166 | 71.76 |
| SM | 35 | 118 | 89 | 0 | 0 | 0 | 64 | 36 | 0 | 0 | 22 | 0 | 14 | 8 | 2722 | 41 | 19 | 3168 | 85.92 |
| SQ | 53 | 185 | 132 | 8 | 11 | 0 | 126 | 110 | 0 | 5 | 135 | 13 | 45 | 72 | 69 | 1,662 | 115 | 2,741 | 60.63 |
| BS | 10 | 278 | 195 | 0 | 0 | 0 | 108 | 122 | 2 | 0 | 59 | 104 | 107 | 36 | 84 | 115 | 1183 | 2403 | 49.23 |
| Tot. | 2127 | 2691 | 3783 | 3438 | 3816 | 6236 | 2831 | 3344 | 3148 | 1638 | 3472 | 4489 | 3462 | 3131 | 3179 | 2385 | 1680 | 54,850 | |
| Prod | 73.95 | 59.16 | 63.12 | 79.87 | 80.03 | 73.26 | 64.35 | 66.29 | 68.39 | 80.83 | 67.77 | 79.57 | 68.48 | 72.56 | 85.62 | 69.69 | 70.42 | | 72.15 |

Note: O = Orchards, CB = Cranberry Bogs, PC = Pasture/Row Crops, DF = Deciduous Forest, CF = Conifer Forest, MF = Mixed Forest, GC = Golf Course, G = Grassland, LD = Low Density Residential, HD = High Density Residential, CI = Commercial/Industrial, DW = Deep Water, SW = Shallow Water, W = Wetland, SM = Salt Marsh, SQ = Sand Quarry, BS = Bare Soil.

from using spectral and temporal (four seasons) dimensions of Landsat data indicate this increase is statistically significant at the 95% level.

Landsat data alone provided high accuracy for all 17 land cover categories when all the available spectral, temporal, and spatial dimensions were used. The producer's and user's accuracies for all land cover types were approximately 90% or higher (Table 4). The three urban land cover classes performed differently, with the highest producer's and user's accuracies in *high density residential* (>90%), moderate producer's and user's accuracies in *commercial/industrial* (approximate 90%), and relatively low producer's and user's accuracies in *low density residential* (<90%). Compared with the other non-urban land cover classes, the produce's and user's accuracies of the three urban land cover types were slightly lower, except the producer's accuracy for *high density residential*. The producer's and user's accuracies for *cranberry bogs*, *deep water*, *and shallow water* were very high (>95%). The best map derived from Landsat (Scenario 7 in Table 2) in the urban areas also showed a high degree of accuracy (Fig. 5b). *Shallow water* was correctly identified in the map. *Low density residential* was labeled accurately without showing any confusion with *conifer forest* and *mixed forest*. *Deciduous forest* was accurately separated from *conifer forest* and *mixed forest*. *Commercial/industrial* was well identified from *high density residential* in downtown Boston. The patch shapes of *forest*, *residential*, *water*, and *golf course* classes matched landscape features. Nonetheless, the three urban land cover types (*commercial/industrial, high density residential,* and *low density residential*) still have problems in this map. *Commercial/industrial* and *high density residential* located in downtown Boston were misclassified as *wetland*, *water*, and *sand quarry*. Many of the *low density residential* sites along Charles River were falsely labeled as *wetland* or *salt marsh*.

### 4.3. Inputs from PALSAR and Landsat

By combining PALSAR and Landsat, four dimensions of inputs are used (Scenario 8 in Table 2). In the spectral dimension, Landsat and PALSAR provides the visible, NIR, SWIR, thermal, and microwave L-band. In the polarimetric dimension, PALSAR provides dual polarization bands. The temporal dimension is provided by the four seasons of Landsat images. The spatial dimension is captured by the eight texture variables calculated for each spectral band from the autumn (September) Landsat image and the PALSAR image with a window size of 9×9 pixels.

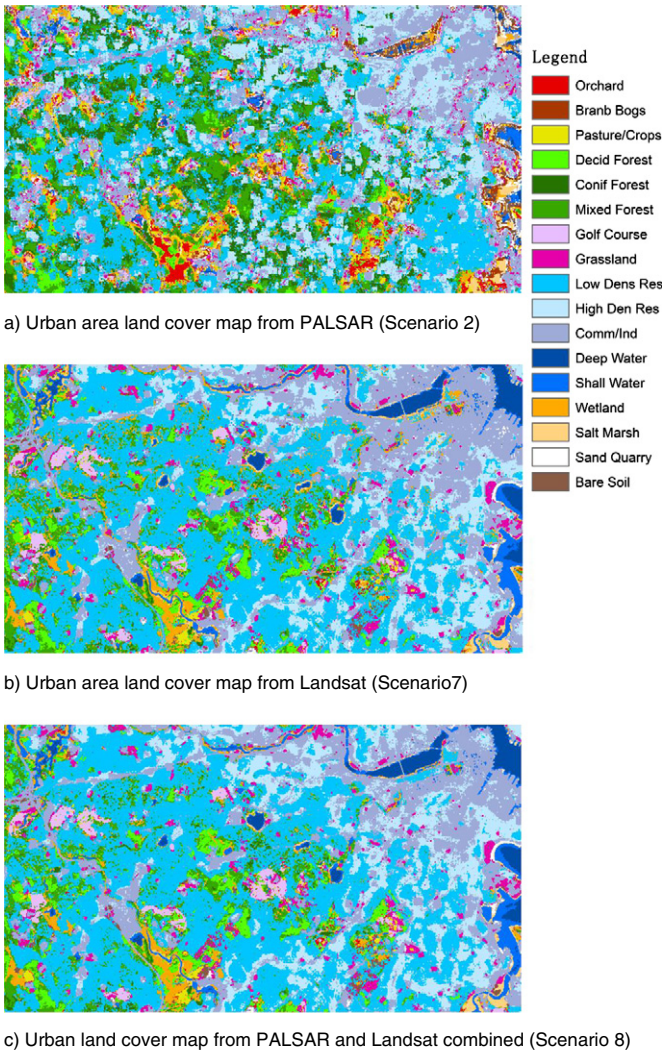


a) Urban area land cover map from PALSAR (Scenario 2)

b) Urban area land cover map from Landsat (Scenario7)

c) Urban land cover map from PALSAR and Landsat combined (Scenario 8)

**Fig. 5.**

**Table 4**
Confusion matrix for 17-categories land cover classification derived from 4 seasons Landsat images and texture measures.

| | O | CB | PC | DF | CF | MF | GC | G | LD | HD | CI | DW | SW | W | SM | SQ | BS | Tot. | User |
|---|---|---|---|---|---|---|---|---|---|---|---|---|---|---|---|---|---|---|---|
| O | 2015 | 0 | 134 | 0 | 0 | 0 | 8 | 44 | 10 | 0 | 14 | 0 | 0 | 0 | 0 | 0 | 1 | 2226 | 90.52 |
| CB | 0 | 2182 | 6 | 0 | 1 | 10 | 0 | 31 | 30 | 0 | 1 | 0 | 0 | 3 | 0 | 0 | 3 | 2267 | 96.25 |
| PC | 91 | 1 | 3264 | 0 | 11 | 0 | 25 | 46 | 47 | 0 | 0 | 0 | 0 | 16 | 0 | 0 | 36 | 3537 | 92.28 |
| DF | 0 | 0 | 0 | 3561 | 0 | 138 | 0 | 0 | 7 | 0 | 0 | 0 | 0 | 8 | 0 | 0 | 2 | 3716 | 95.82 |
| CF | 0 | 5 | 0 | 25 | 3541 | 318 | 0 | 0 | 10 | 0 | 0 | 0 | 0 | 6 | 0 | 0 | 0 | 3905 | 90.68 |
| MF | 0 | 0 | 0 | 234 | 294 | 4923 | 0 | 0 | 8 | 0 | 0 | 0 | 0 | 7 | 0 | 0 | 0 | 5466 | 90.07 |
| GC | 44 | 15 | 35 | 3 | 17 | 3 | 2525 | 56 | 8 | 0 | 0 | 0 | 3 | 0 | 0 | 0 | 0 | 2709 | 93.21 |
| G | 18 | 21 | 70 | 9 | 0 | 0 | 46 | 3190 | 47 | 12 | 0 | 0 | 0 | 2 | 0 | 0 | 32 | 3447 | 92.54 |
| LD | 6 | 1 | 2 | 29 | 0 | 43 | 0 | 10 | 2768 | 59 | 66 | 11 | 18 | 32 | 18 | 1 | 30 | 3094 | 89.46 |
| HD | 0 | 0 | 0 | 0 | 0 | 0 | 0 | 0 | 51 | 1619 | 78 | 0 | 0 | 0 | 1 | 22 | 0 | 1771 | 91.42 |
| CI | 0 | 0 | 0 | 0 | 0 | 44 | 0 | 26 | 86 | 18 | 3335 | 0 | 0 | 0 | 0 | 120 | 53 | 3682 | 90.58 |
| DW | 0 | 0 | 0 | 0 | 0 | 0 | 0 | 0 | 0 | 0 | 0 | 4184 | 156 | 0 | 0 | 0 | 0 | 4340 | 96.41 |
| SW | 0 | 0 | 0 | 0 | 8 | 9 | 0 | 0 | 0 | 0 | 0 | 186 | 3203 | 48 | 7 | 0 | 13 | 3474 | 92.20 |
| W | 0 | 0 | 11 | 18 | 0 | 36 | 0 | 0 | 21 | 0 | 3 | 0 | 68 | 2963 | 10 | 0 | 17 | 3147 | 94.15 |
| SM | 0 | 0 | 0 | 0 | 0 | 9 | 0 | 0 | 0 | 0 | 7 | 0 | 14 | 62 | 2928 | 0 | 7 | 3027 | 96.73 |
| SQ | 0 | 0 | 0 | 0 | 0 | 0 | 0 | 5 | 0 | 0 | 55 | 0 | 0 | 8 | 1 | 2526 | 52 | 2647 | 95.43 |
| BS | 0 | 0 | 83 | 0 | 3 | 18 | 0 | 11 | 32 | 0 | 57 | 0 | 0 | 22 | 0 | 57 | 2112 | 2395 | 88.18 |
| Tot. | 2174 | 2225 | 3605 | 3879 | 3875 | 5551 | 2604 | 3419 | 3125 | 1708 | 3616 | 4381 | 3462 | 3177 | 2965 | 2726 | 2358 | 54850 | |
| Prod | 92.69 | 98.07 | 90.54 | 91.80 | 91.38 | 88.69 | 96.97 | 93.30 | 88.58 | 94.79 | 92.23 | 95.50 | 92.52 | 93.26 | 98.75 | 92.66 | 89.57 | | 92.69 |

Note: O = Orchards, CB = Cranberry Bogs, PC = Pasture/Row Crops, DF = Deciduous Forest, CF = Conifer Forest, MF = Mixed Forest, GC = Golf Course, G = Grassland, LD = Low Density Residential, HD = High Density Residential, CI = Commercial/Industrial, DW = Deep Water, SW = Shallow Water, W = Wetland, SM = Salt Marsh, SQ = Sand Quarry, BS = Bare Soil.

Using all the dimensions available provided by PALSAR and Landsat data, the map accuracy was 93.82% (Fig. 4). Compared with the best classification map from Landsat data, the 1.1% map accuracy increase appears small, but it is statistically significant at the 95% level. There remains only a little more than 6% error after the use of Landsat data, and the addition of PALSAR data helps resolve approximately 15% of the extant error. The producer's and user's accuracies for all 17 land cover types were higher than 90% (Table 5). PALSAR data were particularly helpful in urban land cover type classification when combined with Landsat data. Except for the producer's accuracy for *high density residential*, the producer's and user's accuracy for *low density residential*, *high density residential*, and *commercial/industrial* all increased approximately 2.3–4.6% when PALSAR and Landsat were combined compared to Landsat alone. The inclusion of PALSAR data decreased the producer's accuracy for *high density residential* by 0.3% which is reasonable considering the high producer's accuracy (94.8%) already achieved with Landsat data and the inherent noise in PALSAR data. There were slight increases in producer's and user's accuracies for other non-urban land cover, but the magnitude was very small (Tables 4 and 5). Comparing the land cover map derived from integration of Landsat and PALSAR (Fig. 5c) and the one obtained from Landsat alone (Fig. 5b) in the urban area, we found the basic pattern for the two land cover maps were very similar. The most obvious differences between the two maps were located in the boundary of different land cover types and within the three urban land cover types (Fig. 6). The differences in the urban land cover types showed the special contribution from PALSAR data. The *low density residential* pixels located along Charles River that had been previously misidentified as *wetland* and *salt marsh* were correctly classified as *low and high density residential*. The confusion between *water* and building shadows were greatly reduced. The misclassified *sand quarry* in downtown Boston was also eliminated in the map derived from both Landsat and PALSAR data.

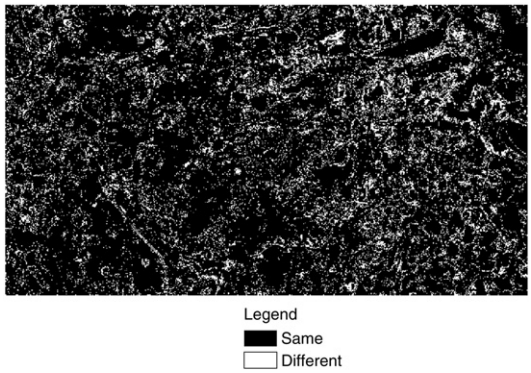


**Fig. 6.** Difference between urban area land cover maps derived from Landsat (Scenario 7), and integration of ALOS and Landsat (Scenario 8).

### 4.4. Importance of the variables

By combining the spectral, polarimetric, temporal, and spatial dimensions of the input data, there are 91 variables for each pixel (Scenario 8 in Table 2). The first twenty-five variables are the four seasons of Landsat images in which the Landsat bands are in the sequence of Band 1, Band 2, Band 3, Band 4, Band 5, and Band 7 (Band 6 only from autumn image). The next two variables are the HH and HV polarization bands from PALSAR. The last sixty-four variables are the eight texture variables computed from each PALSAR (HH and HV) and Landsat spectral bands (six optical bands). The texture variables for each spectral band are in the sequence of mean, variance, homogeneity, contrast, dissimilarity, entropy, second moment, and correlation. The importance of the 91 variables is presented in Fig. 7. Except for the summer (June) image, the NIR band is the most beneficial band in land cover classification, and it works best in the autumn (September) image. The PALSAR HH and HV bands are also helpful, especially the HV band. On the other hand, the most useful variable in the eight texture variables for both PALSAR and Landsat is the mean value for each spectral band at the window size of $9 \times 9$ pixels.

Ideally, each variable used in the classification should provide extra information to the dataset and improve map accuracy. Nevertheless, high correlations between the variables, noise from misregistration of the multi-source data, and the necessity of more parameters to be estimated in the classifier undermine classification accuracy when many variables from different sources are used. Beyond a certain point, the inclusion of more variables may lead to reduced map accuracy, due to the limited number of training samples (Pal, 2006). Therefore, selecting the optimal subset of variables may reduce the computation and at the same time improve the classification accuracy (Chan & Paelinckx, 2008; Pal, 2006; Waske et al., 2010).

We performed a backward elimination technique, that is, iteratively removing the least important variable (importance of each variable is

**Table 5**
Confusion matrix for 17-categories land cover classification derived from combination of Landsat and ALOS data.

| | O | CB | PC | DF | CF | MF | GC | G | LD | HD | CI | DW | SW | W | SM | SQ | BS | Tot. | User |
|---|---|---|---|---|---|---|---|---|---|---|---|---|---|---|---|---|---|---|---|
| O | 2075 | 0 | 103 | 0 | 0 | 0 | 11 | 43 | 10 | 0 | 3 | 0 | 0 | 0 | 0 | 2 | 0 | 2247 | 92.35 |
| CB | 0 | 2181 | 7 | 0 | 0 | 8 | 0 | 43 | 9 | 0 | 0 | 0 | 0 | 2 | 2 | 0 | 9 | 2261 | 96.46 |
| PC | 108 | 0 | 3261 | 0 | 7 | 0 | 22 | 54 | 51 | 0 | 0 | 0 | 0 | 17 | 0 | 0 | 27 | 3547 | 91.94 |
| DF | 0 | 0 | 0 | 3582 | 0 | 96 | 0 | 0 | 7 | 0 | 0 | 0 | 0 | 7 | 0 | 0 | 0 | 3692 | 97.02 |
| CF | 0 | 1 | 0 | 13 | 3524 | 316 | 0 | 0 | 8 | 0 | 0 | 0 | 0 | 8 | 0 | 0 | 0 | 3870 | 91.06 |
| MF | 0 | 0 | 0 | 172 | 314 | 5029 | 0 | 0 | 8 | 0 | 0 | 0 | 0 | 7 | 0 | 0 | 0 | 5530 | 90.94 |
| GC | 17 | 9 | 49 | 17 | 11 | 1 | 2617 | 40 | 17 | 0 | 9 | 0 | 5 | 2 | 0 | 0 | 0 | 2794 | 93.66 |
| G | 29 | 19 | 99 | 18 | 0 | 0 | 51 | 3082 | 43 | 10 | 0 | 0 | 0 | 1 | 8 | 0 | 27 | 3387 | 90.99 |
| LD | 6 | 0 | 0 | 16 | 16 | 35 | 0 | 3 | 2930 | 81 | 41 | 13 | 25 | 5 | 3 | 0 | 20 | 3194 | 91.73 |
| HD | 0 | 0 | 0 | 0 | 0 | 0 | 0 | 0 | 21 | 1645 | 33 | 0 | 0 | 0 | 0 | 15 | 0 | 1714 | 95.97 |
| CI | 0 | 0 | 0 | 0 | 0 | 25 | 0 | 15 | 73 | 5 | 3344 | 0 | 0 | 1 | 0 | 57 | 32 | 3552 | 94.14 |
| DW | 0 | 0 | 0 | 0 | 0 | 0 | 0 | 0 | 0 | 0 | 0 | 4193 | 141 | 0 | 0 | 0 | 0 | 4334 | 96.75 |
| SW | 0 | 0 | 0 | 0 | 3 | 12 | 0 | 0 | 0 | 0 | 0 | 185 | 3249 | 29 | 4 | 0 | 10 | 3492 | 93.04 |
| W | 1 | 0 | 2 | 7 | 0 | 32 | 0 | 0 | 7 | 0 | 7 | 0 | 58 | 2940 | 1 | 0 | 4 | 3059 | 96.11 |
| SM | 0 | 0 | 0 | 0 | 0 | 11 | 0 | 0 | 0 | 0 | 0 | 0 | 12 | 8 | 3118 | 0 | 7 | 3156 | 98.80 |
| SQ | 0 | 0 | 0 | 0 | 0 | 2 | 0 | 2 | 0 | 0 | 33 | 0 | 0 | 16 | 0 | 2535 | 52 | 2640 | 96.02 |
| BS | 0 | 0 | 87 | 0 | 0 | 18 | 0 | 12 | 0 | 0 | 30 | 0 | 0 | 25 | 0 | 56 | 2153 | 2381 | 90.42 |
| Tot. | 2236 | 2210 | 3608 | 3825 | 3875 | 5585 | 2701 | 3294 | 3184 | 1741 | 3500 | 4391 | 3490 | 3068 | 3136 | 2665 | 2341 | 54850 | |
| Prod | 92.80 | 98.69 | 90.38 | 93.65 | 90.94 | 90.04 | 96.89 | 93.56 | 92.02 | 94.49 | 95.54 | 95.49 | 93.09 | 95.83 | 99.43 | 95.12 | 91.97 | | 93.82 |

Note: O = Orchards, CB = Cranberry Bogs, PC = Pasture/Row Crops, DF = Deciduous Forest, CF = Conifer Forest, MF = Mixed Forest, GC = Golf Course, G = Grassland, LD = Low Density Residential, HD = High Density Residential, CI = Commercial/Industrial, DW = Deep Water, SW = Shallow Water, W = Wetland, SM = Salt Marsh, SQ = Sand Quarry, BS = Bare Soil.

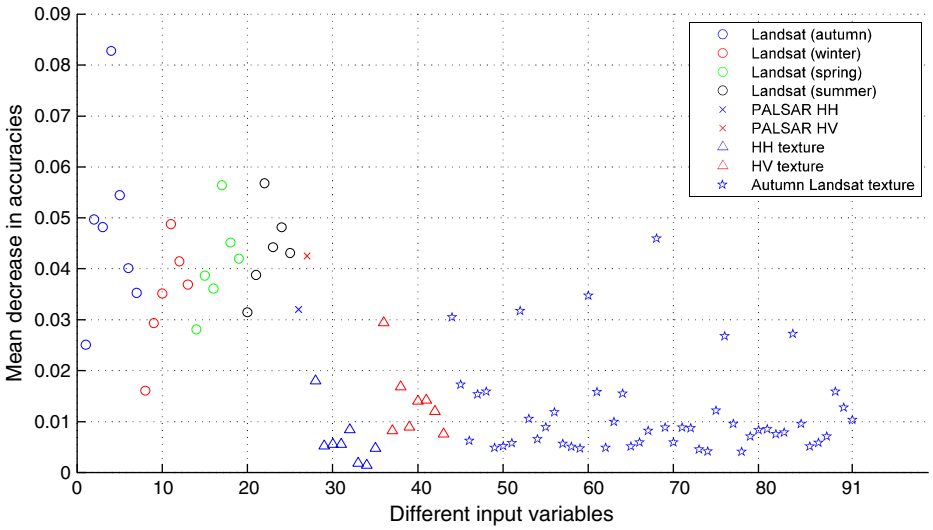


**Fig. 7.** Importance of the 91 different input variables from all available dimensions by combing Landsat and PALSAR data.

reevaluated at each iteration) and calculating the overall map accuracy using the remaining variables (Fig. 8). The overall accuracies decreased very slightly when removing the first 81 least important variables. Overall accuracies started to decrease quickly when there are only 15 variables left. In Fig. 8, the most important 15 variables are removed in the order of mean Band 3 (autumn Landsat texture), mean Band 4 (autumn Landsat texture), Band 2 (summer Landsat), Band 7 (spring Landsat), Band 3 (summer Landsat), Band 4 (spring Landsat), Band 2 (spring Landsat), HV polarization, Band 2 (autumn Landsat), Band 5 (winter Landsat), Band 5 (summer Landsat), Band 3 (summer Landsat), Band 4 (autumn Landsat), Band 3 (autumn Landsat), and Band 5 (autumn Landsat).

## 5. Discussion and conclusions

We evaluated the importance of different dimensions of the input data and the strengths of different sensors in urban and peri-urban land cover classification. When using PALSAR data only, the dual polarization bands resulted in low classification accuracy. By adding the spatial dimension of PALSAR data, overall classification accuracy improved substantially. When using a single Landsat image from autumn (September), higher overall classification accuracy was observed. The addition of the temporal dimension (four seasons of Landsat images) and the spatial dimension further increased the overall classification accuracy. By combining Landsat and PALSAR and using all available dimensions, we achieved the highest overall classification accuracy.

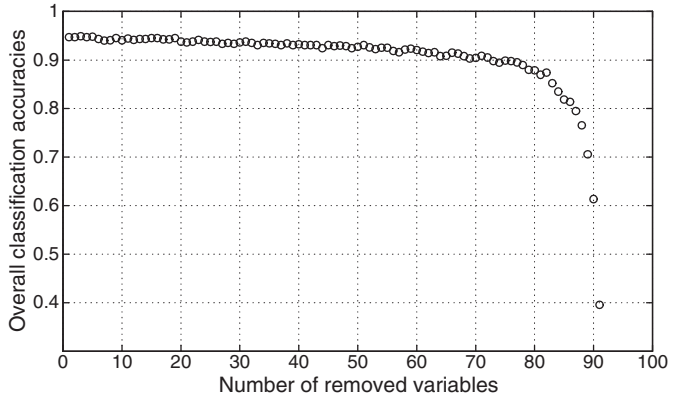


**Fig. 8.** Overall classification accuracies based on backward elimination of the least important variable.

Though the addition of PALSAR only increased the overall accuracy by 1.1%, this improvement was mostly from better discrimination of the three urban land cover types. If we only combine the spectral bands from PALSAR image and an autumn (September) Landsat image, there is a 3% increase in overall accuracy compared with using the Landsat image. Moreover, the PALSAR texture variables can add another 2.2% in overall accuracy even after using multitemporal Landsat and the dual polarization bands from PALSAR.

The different variables from each dimension of the data all contribute to the improved classification accuracy (Fig. 8). Though some of the variables contribute relatively little, the trend is straightforward: more independent input data results in higher classification accuracy. In this study, RFC showed its strong ability in classifying a dataset with many variables (some of which may be highly correlated) without variable deletion. For an advanced classifier like RFC, as long as the additional variable can provide extra information, assuming the influence of noise is relatively small, the classification accuracy should improve. The spectral bands from the autumn (September) Landsat image are the most important variables, which is probably due to the fact that it is the time when deciduous and evergreen vegetation shows the greatest difference. Due to the interchangeability of the cross polarization, HV polarization is can provide unique information about surface features which might be lost when using like polarizations (HH and VV) (Sheoran et al., 2009). Noise from misregistration is always a big issue when classifying multiple bands from different dates and different sensors. The mean value computed from the texture variables can reduce this problem and therefore increases map accuracy. Note that the overall accuracy achieved (89%) by using only 15 important variables is significantly higher than scenario 6 (Table 2) which used 25 multi-temporal Landsat spectral bands.

It is important to note that the reference classes are defined based on a long history of land cover classification using Landsat. If a different set of classes were used that are defined on the basis of surface characteristics that more strongly influence radar data, such as physical structure, then the relative importance of Landsat and PALSAR may change.

In conclusion, including more dimensions of input data and more sensors that complement each other improves urban and peri-urban land cover classification accuracy. The spectral, polarimetric, temporal, and spatial dimensions all contribute to increased classification accuracies. The additional temporal and spatial dimensions of Landsat images are of great importance for improving classification accuracies for all land cover types. The land cover map derived using only the dual polarization L-band PALSAR data has low map accuracy. The spatial

dimension of the PALSAR image helps, but it is still less accurate than simply using an autumn (September) Landsat image. The best classification result is derived from the combination of Landsat and PALSAR data using all available dimensions. The inclusion of PALSAR with Landsat data improved the overall classification significantly by 1.1%, mostly improving the three urban land cover types (*low density residential*, *high density residential* and *commercial/industrial*). Selecting a few (15 variables in this study) important variables from different dimensions of input data can result in relatively high accuracy, but it is still lower than using all available data.

## References


Amarsaikhan, D., & Douglas, T. (2004). Data fusion and multisource image classification. *International Journal of Remote Sensing*, *25*(17), 3529–3539.

Anys, H., Bannari, A., He, D. C., & Morin, D. (1994). Texture analysis for the mapping of urban areas using airborne MEIS-II images. *Proceedings of the First International Airborne Remote Sensing Conference and Exhibition, Strasbourg, France*, *Vol. 3*. (pp. 231–245).

Archer, K. J., & Kimes, R. V. (2008). Empirical characterization of random forest variable importance measures. *Computational Statistics & Data Analysis*, *52*(4), 2249–2260.

Augusteijin, M. F., & Warrender, C. E. (1998). Wetland classification using optical and radar data and neural network classification. *International Journal of Remote Sensing*, *19*(8), 1545–1560.

Baraldi, A., & Panniggiani, F. (1995). A refined gamma MAP SAR speckle filter with improved geometrical adaptivity. *IEEE Transactions on Geoscience and Remote Sensing*, *33*, 1245–1257.

Bischof, H., Schneider, W., & Pinz, A. J. (1992). Multispectral classification of Landsat images using neural networks. *IEEE Transactions on Geoscience and Remote Sensing*, *30*(3), 482–490.

Blaes, X., Vanhalle, L., & Defourny, P. (2005). Efficiency of crop identification based on optical and SAR image time series. *Remote Sensing of Environment*, *96*, 352–365.

Breiman, L. (2001). Random forests. *Machine Learning*, *45*, 5–32.

Breunig, J. (2003). Losing ground: at what cost? Changes in land use and their impact on habitat, biodiversity, and ecosystem services in Massachusetts. *Summary Report* (pp. 1–24). (3rd Edition). : Massachusetts Audobon Society.

Bruzzone, L., Chi, M., & Marconcini, M. (2006). A novel transductive SVM for semisupervised classification of remote-sensing images. *IEEE Transactions on Geoscience and Remote Sensing*, *44*(11), 3363–3373.

Butler, B. J. (2008). *Forest ownership patterns are changing.* National Woodlands. http://www.nrs.fs.fed.us/pubs/jrnl/2008/nrs_2008_butler_001.pdf (accessed December 2, 2010).

Chan, J. C., & Paelinckx, D. (2008). Evaluation of Radom Forest and Adaboost tree-based ensemble classification and spectral band selection for ecotope mapping using airborne hyperspectral imagery. *Remote Sensing of Environment*, *112*, 2999–3011.

Chen, C. T., Chen, K. S., & Lee, J. S. (2003). The use of fully polarimetric information for the fuzzy neural classification of SAR image. *Transactions on Geoscience and Remote Sensing*, *41*(9), 352–365.

Chica-Olmo, M., & Abarca-Hernandez, F. (2000). Computing geostatistical image texture for remotely sensed data classification. *Computers and Geosciences*, *26*, 373–383.

Chust, G., Durcot, D., & Pretus, J. L. L. (2004). Land cover discrimination potential of radar multitemporal series and optical multispectral images in a Mediterranean cultural landscape. *International Journal of Remote Sensing*, *25*(17), 3513–3528.

Cloude, S. R., & Potter, E. (1997). An entropy based classification scheme for land applications of polarimetric SAR. *Transactions on Geoscience and Remote Sensing*, *35*(1), 68–78.

Corbane, C., Faure, J., Baghdadi, N., Villeneuve, N., & Petit, M. (2008). Rapid urban mapping using SAR/optical imagery synergy. *Sensors*, *8*, 7125–7143.

Davis, P. (2007). Rhode Island forests are losing ground. *Providence Journal* (2007, August 20) Online:. http://www.projo.com/business/content/NOTREES_08-19-07_V72S7BR.2d4b367.html (accessed December 2, 2010)

Defries, R. S., & Townshend, J. R. G. (1994). NDVI-derived land cover classification at global scale. *International Journal of Remote Sensing*, *15*(17), 3567–3586.

Dekker, R. J. (2003). Texture analysis and classification of ERS SAR images for Map updating of urban areas in the Netherland. *Geoscience and Remote Sensing*, *41*(9), 1950–1958.

Dell'Acqua, F., & Gamba, P. (2003). Texture-based characterization of urban environments on satellite SAR images. *IEEE Transactions on Geoscience and Remote Sensing*, *41*(1), 153–159.

Dell'Acqua, F., & Gamba, P. (2006). Discriminating urban environments using multiscale texture and multiple SAR images. *International Journal of Remote Sensing*, *27*(18), 3797–3812.

DeNormandie, J. (2009). Losing ground: beyond the footprint: Patterns of development and their impact on the nature of Massachusetts. (4th Edition). : Massachusetts Audubon Society.

Fielding, A. H., & Bell, A. J. F. (1997). A review of methods for the assessment of prediction errors in conservation presence/absence models. *Environmental Conservation*, *24*(1), 38–49.

Franklin, S. E., & Peddle, D. R. (1990). Classification of SPOT HRV imagery and texture features. *International Journal of Remote Sensing*, *11*, 551–556.

Franklin, S. E., Hall, R. J., Moskal, L. M., Maudie, A. J., & Lavigne, M. B. (2000). Incorporating texture into classification of forest species composition from airborne multispectral images. *International Journal of Remote Sensing*, *21*(1), 61–79.

Friedl, M. A., Menashe, D. S., Tan, B., Schneider, A., Ramankutty, N., Sibley, A., et al. (2010). MODIS collection 5 global land cover: Algorithm refinements and characterization of new datasets. *Remote Sensing of Environment*, *114*, 168–182.

Ghimire, B., Rogan, J., & Miller, J. (2010). Contextural land-cover classification: incorporating spatial dependence in land-cover classification models using random forests and the Getis statistic. *Remote Sensing Letters*, *1*(1), 45–54.

Gislason, P. O., Benediktsson, J. A., & Sveinsson, J. R. (2006). Random forests for land cover classification. *Pattern Recognition Letters*, *27*(4), 294–300.

Gong, P., & Howarth, P. J. (1992). Frequency-based contextual classification and gray-level vector reduction for land-use identification. *Photogrammetric Engineering and Remote Sensing*, *58*, 423–437.

Gopal, S., Woodcock, C. E., & Strahler, A. (1999). Fuzzy neural classification of global land cover from a 1 degree AVHRR Data Set. *Remote Sensing of Environment*, *67*, 230–243.

Guerschman, J. P., Paruelo, J. M., Bella, C. D. I., Giallorenzi, M. C., & Pacin, F. (2003). Land cover classification in the Argentine Pampas using multi-temporal Landsat TM data. *International Journal of Remote Sensing*, *24*(17), 3381–3402.

Ham, J., Chen, Y., Crawford, M. M., & Ghosh, J. (2005). Investigation of random forest framework for classification of hyperspectral data. *IEEE Transactions on Geoscience and Remote Sensing*, *43*(3), 492–501.

Hansen, M. C., Defries, R. S., Townshend, J. R. G., & Sohlberg, R. (2000). Global land cover classification at 1 km spatial resolution using a classification tree approach. *International Journal of Remote Sensing*, *21*(6 & 7), 1331–1364.

Huang, C., Davis, L. S., & Townshend, J. R. (2002). An assessment of support vector machines for land cover classification. *International Journal of Remote Sensing*, *23*(4), 725–749.

Jung, M., Henkel, K., Herold, M., & Churkina, G. (2006). Exploiting synergies of global land cover products for carbon cycle modeling. *Remote Sensing of Environment*, *101*(4), 534–553.

Kellndorfer, J. M., Pierce, L. E., Dobson, M. C., & Ulaby, F. T. (1998). Toward consistent regional-to-global-scale vegetation characterization using orbital SAR systems. *IEEE Transactions on Geoscience and Remote Sensing*, *36*, 1396–1411.

Kuplich, T. M., Freitas, C. C., & Soares, J. V. (2000). The study of ERS-1 SAR and Landsat TM synergism for land use classification. *International Journal of Remote Sensing*, *21*(10), 2101–2111.

Lark, R. M., & Stafford, J. V. (1997). Classification as a first step in the interpretation of temporal and spatial variation of crop yield. *The Annals of Applied Biology*, *130*(1), 111–121.

Le Toan, T., Laur, H., Mougin, E., & Lopes, A. (1989). Multitemporal and dual-polarization observations of agricultural vegetation covers by X-band SAR images. *Geoscience and Remote Sensing*, *27*, 709–718.

Lee, J. S., Grunes, M. R., & Kwork, R. (1994). Classification of multi-look polarimetric SAR imagery based on complex Wishart distribution. *International Journal of Remote Sensing*, *15*(11), 2299–2311.

Li, H., & Chen, W. (2005). A rule-based method for mapping Canada's wetlands using optical, radar and DEM data. *International Journal of Remote Sensing*, *26*(22), 5051–5069.

Lu, D., & Batistella, M. (2005). Exploring TM image texture and its relationships with biomass estimation in Rondônia, Brazilian Amazon. *Acta Amazonica*, *35*(2), 249–257.

Lu, D., & Weng, Q. (2007). A survey of image classification methods and techniques for improving classification performance. *International Journal of Remote Sensing*, *28*(5), 823–870.

Masek, J. G., Vermote, E. F., Saleous, N., Wolfe, R., Hall, E. F., Huemmrich, F., et al. (2006). A Landsat surface reflectance data set for North America, 1990–2000. *Geoscience and Remote Sensing Letters*, *3*, 68–72.

Michelson, D. B., Liljeberg, B. M., & Pilesjo, P. (2000). Comparison of algorithms for classifying Swedish landcover using Landsat TM and ERS-1 SAR data. *Remote Sensing of Environmental*, *71*, 1–15.

NCDA (National Climate Data Center) (2008). *Satellite and information service.* : National Oceanic and Atmospheric Administration and National Climate Data Center November 10. http://lwf.ncdc.noaa.gov (accessed December 2, 2010).

Nowak, D. J., & Walton, J. T. (2005). Projected urban growth (2000–2050) and its estimated impact on the US forest resource. *Journal of Forestry*, *103*(8), 383–389.

Pal, M. (2005). Random forest classifier for remote sensing classification. *International Journal of Remote Sensing*, *26*(1), 217–222.

Pal, M. (2006). Support vector machine-based feature selection for land cover classification: A case study with DAIS hyperspectral data. *International Journal of Remote Sensing*, *27*(14), 2877–2894.

Pellizzeri, T. M., Gamba, P., Lombardo, P., & Acqua, F. D. (2003). Multitemporal/multiBand SAR classification of urban areas using spatial analysis: statistical versus neural kernel-based approach. *Geoscience and Remote Sensing*, *41*(10), 2338–2353.

Pesaresi, M. (2000). Texture analysis for urban pattern recognition using fine-resolution panchromatic satellite imagery. *Geographical and Environmental Modelling*, *4*(1), 43–63.

Prasad, A. M., Lverson, L. R., & Liaw, A. (2006). Newer classification and regression tree techniques: Bagging and random forests for ecological prediction. *Ecosystems*, *9*, 181–199.

Puissant, A., Hirsch, J., & Weber, C. (2005). The utility of texture analysis to improve per-pixel classification for high to very high spatial resolution imagery. *International Journal of Remote Sensing*, *26*(4), 733–745.

Quegan, S., Toan, T. L., Yu, J. J., Ribbes, F., & Floury, N. (2000). Multitemporal ERS SAR analysis applied to forest mapping. *Geoscience and Remote Sensing*, *38*(2), 741–753.

Rogan, J., & Chen, d. M. (2004). Remote sensing technology for mapping and monitoring land-cover and land-use change. *Progress in Planning*, *61*(4), 301–325.

Rogan, J., Franklin, J., Stow, D., Miller, J., Woodcock, C., & Roberts, D. (2008). Mapping land-cover modifications over large areas: A comparison of machine learning algorithms. *Remote Sensing of Environment*, *112*, 2272–2283.

Rogan, J., Bumbarger, N., Kulakowski, D., Christman, Z., Runfola, D., & Blanchard, S. D. (2010). Improving forest type discrimination with mixed lifeform classes using fuzzy classification thresholds informed by field observations. *Canadian Journal of Remote Sensing*, *36*(6), 699–708.

Rosenqvist, A., Shimada, M., Ito, N., & Watanabe, M. (2007). ALOS PALSAR: A pathfinder mission for global-scale monitoring of the environment. *IEEE International Geoscience and Remote Sensing Symposium* (pp. 3307–3316).

Rott, H. (1994). Thematic studies in alpine areas by means of polarimetric SAR and opticalimagery. *Advances in Space Research*, *14*(3), 217–226.

SARScape User Manual. (2009). SARMAP, Inc.

Schotten, C. G. J., Rooy, W. W. L., & Janssen, L. L. F. (1995). Assessment of capabilities of multi-temporal ERS-1 SAR data to discriminate between agricultural crops. *International Journal of Remote Sensing*, *16*(14), 2619–2637.

Shaban, M. A., & Dikshit, O. (2001). Improvement of classification in urban areas by the use of textural features: the case study of Lucknow city, Uttar Pradesh. *International Journal of Remote Sensing*, *22*, 565–593.

Sheoran, A., Haack, B., & Sawaya, S. (2009). Land cover/use classification using optical and quad polarization radar imagery. *ASPRS 2009 Annual Conference, Baltimore, Maryland*.

Shimabukuro, Y. E., & Smith, J. A. (1991). The least-squares mixing models to generate fraction images derived from remote sensing multispectral data. *IEEE Transactions on Geoscience and Remote Sensing*, *29*(1), 16–20.

Shupe, S. M., & Marsh, S. E. (2004). Cover-and density-based vegetation classification of the sonorant desert using Landsat TM and ERS-1 SAR imagery. *Remote Sensing of Environment*, *93*, 131–149.

Simard, M., Saatchi, S. S., & Grandi, G. D. (2000). The use of decision tree and multiscale texture for classification of JERS-1 SAR data over tropical forest. *Geoscience and Remote Sensing*, *38*(5), 2310–2321.

Solberg, A. H. S., Jain, A. K., & Taxt, T. (1994). Multisource classification, of remotely sensed data: Fusion of Landsat TM and SAR images. *Geoscience and Remote Sensing*, *32*(4), 768–778.

Steven, E. F., & Derek, R. P. (1990). Classification of SPOT HRV imagery and texture features. *International Journal of Remote Sensing*, *11*, 551–556.

Strahler, A. H. (1980). The use of prior probabilities in maximum likelihood classification of remote sensing data. *Remote Sensing of Environment*, *10*, 135–163.

Toll, D. L. (1985). Analysis of digital LANDSAT MSS and SEASAT SAR data for use in discriminate land cover at the urban fringe of Denver, Colorado. *International Journal of Remote Sensing*, *6*(7), 1209–1229.

Tucker, C. J., Townshend, J. R. G., & Goff, T. E. (1985). African land-cover classification using satellite data. *Science*, *227*(4685), 369–375.

Ulaby, F. T., Kouyate, F., Brisco, B., & Williams, T. H. L. (1986). Textural information in SAR Images. *Transaction on Geoscience and Remote Sensing*, *GE-24*(2), 235–245.

Vermote, E. F., El Saleous, N., Justice, C. O., Kaufman, Y. J., Privette, J. L., Remer, L., et al. (1997). Atmospheric correction of visible to middle-infrared EOS-MODIS data over land surfaces: Background, operational algorithm, and validation. *Journal of Geophysical Research*, *102*, 17131–17141.

Wang, F. (1990). Fuzzy supervised classification of remote sensing images. *IEEE Transactions on Geoscience and Remote Sensing*, *28*(2), 194–201.

Waske, B., Linden, S., Benediktsson, J. A., & Hostert, P. (2010). Sensitivity of support vector machines to random feature selection in classification of hyperspectral data. *IEEE Transactions on Geoscience and Remote Sensing*, *48*(7), 2880–2889.

Wolter, P. I., Mladenoft, D. S., & Crow, T. R. (1995). Improved forest classification in the northern lake states using multi-temporal Landsat imagery. *Photogrammetry Engineering & Remote Sensing*, *61*(9), 1129–1143.

Woodcock, C. E., Macomber, S. A., Pax-Lenney, M., & Cohen, W. B. (2001). Large area monitoring of temperate forest change using Landsat data: Generalization across sensors, time and space. *Remote Sensing of Environment*, *78*(1–2), 194–203.

Zhu, Z., & Woodcock, C.E. submitted for publication. Object-based cloud and cloud shadow detection in Landsat imagery. *Remote Sensing of Environment*.